Acoustic signal and noise changes in the Beaufort Sea Pacific Water duct under anticipated future acidification of Arctic Ocean waters

Timothy F. Duda

Citation: The Journal of the Acoustical Society of America **142**, 1926 (2017); doi: 10.1121/1.5006184
View online: https://doi.org/10.1121/1.5006184
View Table of Contents: https://asa.scitation.org/toc/jas/142/4
Published by the Acoustical Society of America

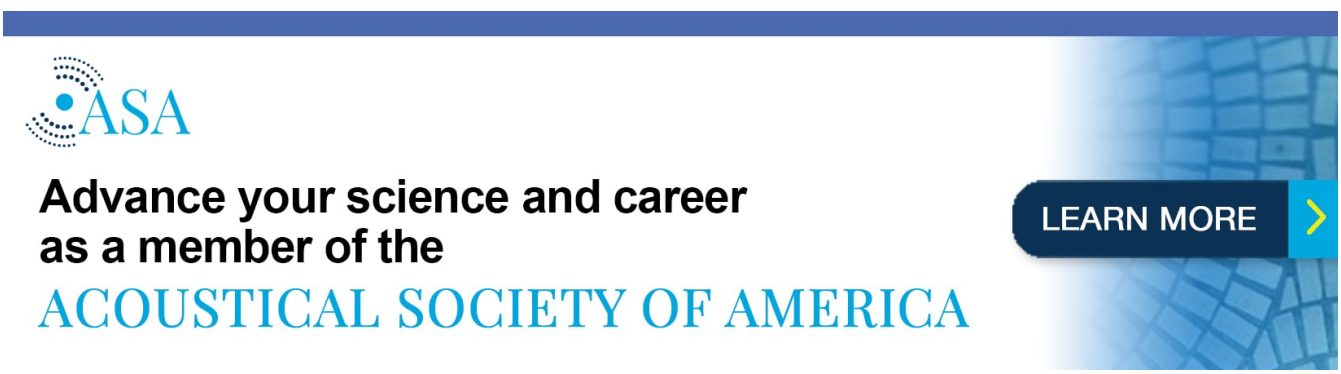

Acoustic signal and noise changes in the Beaufort Sea Pacific Water duct under anticipated future acidification of Arctic Ocean waters

Timothy F. Duda[a)]
Applied Ocean Physics and Engineering Department, Woods Hole Oceanographic Institution, Woods Hole, Massachusetts 02543, USA

(Received 5 May 2017; revised 29 August 2017; accepted 21 September 2017; published online 9 October 2017)

It is predicted that Arctic Ocean acidity will increase during the next century as a result of carbon dioxide accumulation in the atmosphere and migration into ocean waters. This change has implications for sound transmission because low-*p*H seawater absorbs less sound than high-*p*H water. Altered *p*H will affect sound in the 0.3−10 kHz range if the criterion is met that absorption is the primary cause of attenuation, rather than the alternatives of loss in the ice or seabed. Recent work has exploited sound that meets the criterion, sound trapped in a Beaufort Sea duct composed of Pacific Winter Water underlying Pacific Summer Water. Arctic *p*H is expected to drop from 8.1 to 7.9 (approximately) over the next 30−50 yr, and effects of this chemical alteration on the intensity levels of this ducted sound, and on noise, are examined here. Sound near 900 Hz is predicted to undergo the greatest change, traveling up to 38% further. At ranges of 100−300 km, sound levels from a source in the duct may increase by 7 dB or more. Noise would also increase, but noise is ducted less efficiently, with the result that 1 kHz noise is predicted to rise approximately 0.5 dB.
 https://doi.org/10.1121/1.5006184

[JAC] Pages: 1926–1933

I. INTRODUCTION

It is well documented that the carbon dioxide concentration of the atmosphere is increasing, and will continue to do so for the next century or more. In response, the ocean is taking up CO_2, with a result that the *p*H is declining (Doney *et al.,* 2009). Because long-term alterations of ocean *p*H stem from changes in carbon dioxide flux from the atmosphere, predicted future *p*H decreases are expected to begin near the ocean surface in most areas and penetrate downward (Feely *et al.,* 2004; Caldeira and Wickett, 2005). Because the absorption of sound at frequencies below about 5 kHz is dominantly caused by *p*H-dependent borate ion chemistry (Francois and Garrison, 1982a), the result will be that sound at those frequencies will travel further in situations where the volume absorption is a dominant player in transmission loss. At higher frequencies the *p*H-independent manganese sulfate absorption dominates and the *p*H reduction will have negligible impact. At frequencies below a few hundred hertz there is minimal absorption, and little change in sound propagation is predicted (Udovydchenkov *et al.,* 2010; Reeder and Chiu, 2010; Joseph and Chui, 2010). In situations where sound interaction with ice cover and/or the seafloor dominates transmission loss, the absorption effects are also less important. However, there is a propagation scenario that will be *p*H-dependent: sound at 400−5000 Hz trapped in a sound channel (duct) that that does not interact with boundaries. This precise scenario has been used for under-ice navigation and data transmission in the Beaufort Sea (Webster *et al.,* 2015; Freitag *et al.,* 2015), so the effect has relevance for human operations and the future soundscape in that area. The vertically limited duct in the Beaufort Sea that was exploited for those systems, which operated around 900 Hz, provides unique conditions for signal enhancement by *p*H reduction. Effects of altered *p*H on Beaufort Sea duct propagation are examined in this paper.

One way to quantify the effect of decreasing *p*H on ducted sound uses the fact that, with reduced absorption, sound will travel further from its source before reaching a given attenuation value. This has obvious implications for both known signals and the noise field. Here, we model both signals and noise in present conditions and in forecasted future conditions. Signals are predicted to travel further (or have higher intensity at a given distance), and noise is predicted to also increase, but to a lesser degree, resulting in increased signal to noise ratio (SNR). Computational modeling of sound transmission is used here to examine the ducting. Sound at 900 Hz is used because that is the frequency of the operational system, and there are recent Arctic measurements of average noise levels in that band (Kinda *et al.,* 2013) and transient noise from ice cracking, fracturing, shearing, and ridging (Kinda *et al.,* 2015) to guide the noise modeling. The computational modeling results support the use of a simple model of ducted propagation that can be extended to other frequencies. The simple propagation model is also used for noise studies by modeling noise as sound from many sources.

The field-demonstrated efficient propagation of 900-Hz ducted sound is an important aspect of this work. It turns out that 900 Hz is near the center of the band of *p*H sensitivity, as shown later in the paper, but that is not why the frequency

a)Electronic mail: tduda@whoi.edu

was used in the systems, it is a coincidence. It is known that the largest percentage of *p*H-driven reduction of absorption will be at the lowest frequencies, reaching as high as 40% reduction below 500 Hz (Hester *et al.*, 2008; Brewer and Hester, 2009). However, absorption decreases with decreasing frequency and is very low below a few hundred hertz, so *p*H changes would have negligible resultant effect on propagation in this band. (This is because reducing a number that is near zero produces a number that is also near zero.) This means that signal and noise fields at those frequencies are only weakly controlled by absorption, and are unlikely to change much, with small changes in low-frequency noise levels predicted in a few papers (Reeder and Chiu, 2010; Joseph and Chiu, 2010; Udovydchenkov *et al.*, 2010). On the other hand, sounds at high frequencies are more strongly absorbed by $MgSO_4$ than borate and changes in the *p*H-dependent borate contribution are masked by the dominant $MgSO_4$ absorption. Sound near 900 Hz is in the *p*H-sensitive band between these two end points where *p*H changes do not have much effect.

The paper is structured in this way: Section II presents computational model results for 900-Hz ducted propagation in the Beaufort Sea, and uses the results to defend a simple propagation model. Section III presents a future *p*H prediction for the Arctic Ocean, and shows absorption as a function of frequency for present and predicted future *p*H conditions. Section IV compares current and future ducted propagation of signals at many frequencies. Section V describes a noise model and shows noise predictions. Section VI discusses SNR. Section VII concludes.

II. DUCTED BEAUFORT SEA PROPAGATION

Waters of the Beaufort Gyre are uniquely stratified, with, from the top down: a cold and less saline surface water mass, a warmer but saltier layer of Pacific Summer Water (PSW) entering through the Bering Strait (Pickart, 2004; Spall *et al.*, 2008), a cooler layer of Pacific Winter Water (PWW) with similar geographic origin (Pickart *et al.*, 2005; Itoh *et al.*, 2012), the slightly warmer and saltier Atlantic Water, and cold the Arctic Deep Water. Figure 1(a) shows the conditions. A sound-speed minimum in the PWW creates a duct, sometimes called the Beaufort Lens. Sound propagating at low angle with respect to horizontal from a source in the duct at ∼150 m depth will be trapped and will not be subject to surface ice and/or surface wave scattering loss mechanisms. Eddies of variable temperature and salinity may move from the Alaska north shelf into the gyre (Spall *et al.*, 2008; Itoh *et al.*, 2012) and alter the duct, but their effect on duct continuity is not well known at this time. The previously mentioned acoustic navigation system for undersea platforms has leveraged the ducting conditions (Freitag *et al.*, 2015; Webster *et al.*, 2015), and data from the system demonstrate that 900-Hz sound can travel hundreds of kilometers in the duct. The characteristics of the duct in the future ocean are not known. However, it is anticipated that Pacific Summer Water will increase in volume and/or heat content, so the duct is unlikely to disappear.

Figure 1(b) shows parabolic equation model results for 900-Hz CW signals in the duct. Figure 2 shows model results for pulses with 50-Hz bandwidth. At each range of each simulation one of two surface conditions is implemented, the first being a flat pressure-release surface (flat air/water interface), the second being an uppermost layer intended to mimic ice using the complex-density method (Zhang and Tindle, 1995). The ice can have a flat underside or a variable-height (rough) underside. The ice compressional wave attenuation is 0.5 dB/m, shear wave attenuation 2 dB/m, compressional wave speed 2500 m/s, shear wave speed 1200 m/s, and the ice density is 0.910 g/ml. The complex density that results is 0.356 + 0.994i.

Including the complex-density layer between the air and the water can only approximate the effect of ice on the sound

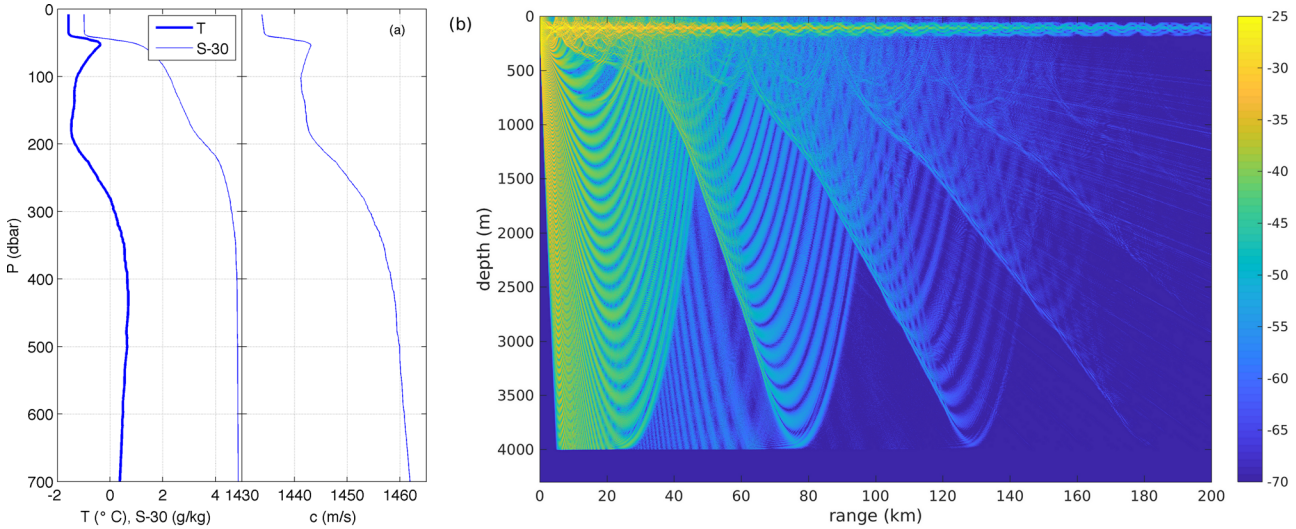

FIG. 1. (Color online) (a) (Left) Upper water column temperature *T* and salinity *S* are shown from one profile from instrument ITP78 suspended from the ice. ITP78 was deployed on a 1.7 m thick ice floe in the Beaufort Sea on March 11, 2014 at 74° 21.6 N, 135° 8.3 W (Woods Hole Oceangr. Inst., 2007). Computed sound speed is also shown. (b) (Right) A plot of 900-Hz transmission loss (dB) versus range and depth is shown for a source in the duct (110 m depth). An ice cover with a rough bottom is used as described in the text. Cylindrical spreading loss is removed in the plot, so that attenuation seen in the duct is due to absorption computed for *p*H 8.1.

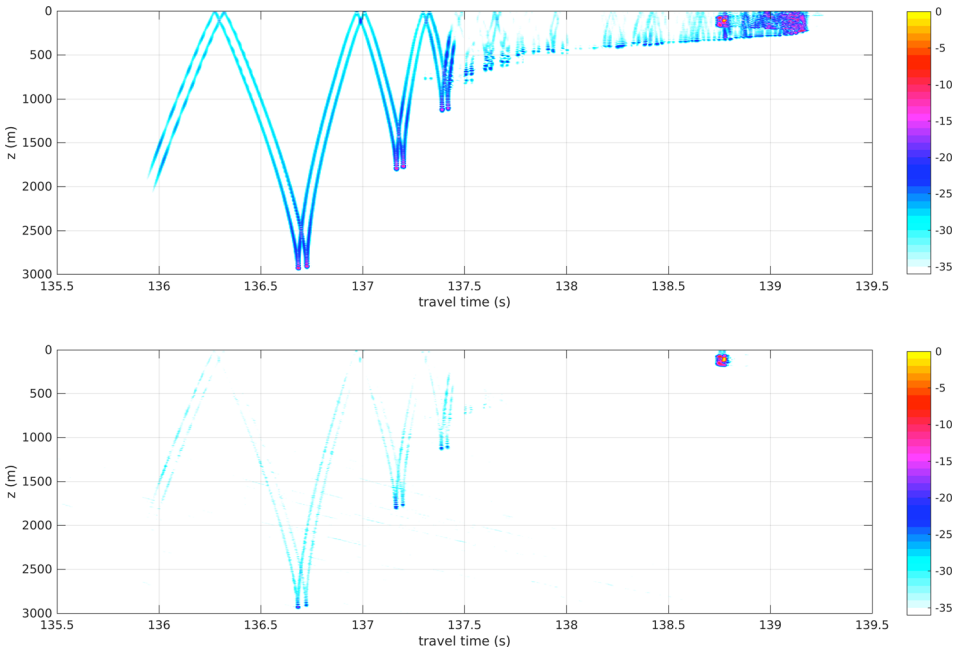

FIG. 2. (Color online) Two impulse responses are shown at 200 km range for a 110-m depth 900-Hz source with 50-Hz bandwidth in the duct conditions plotted in Fig. 1. At the top is the result using a flat sea surface, below is the result using simulated rough ice on top. The maximum level (0 dB in the figure) for the top panel is −88.7 dB. Sound arriving at 138.75 s that is trapped in the duct is not affected by the ice, although it will coexist with and interfere with surface-reflected sound in the no-ice case.

field. First of all, the complex density method is for a half-space and will not include effects of the air−ice boundary. This is not the only compromising factor in this approximation, and the discrepancy that it may cause is not judged to be major with respect to other sources of uncertainty in the ice cover modeling. For example, brine channels and other inhomogeneities in the ice are also not included, so any homogeneous ice treatment will give an approximate result. The complex density that was used gives a reflection coefficient that drops quickly from unity at grazing incidence to a minimum of 0.15 at 35 deg, then rises to a near-steady level near 0.74 from 60 to 90 deg. This reflectivity drops from unity more immediately than the reflectivity at 1000 Hz calculated by Yew and Weng (1987), but is higher at the minimum than the Yew and Weng reflectivity. In addition, the reflectivities of ∼0.74 at near-normal incidence are much higher than those computed by Yew and Weng, which are −8 to −10 dB. The reflectivity curve for the ice underside in another recent study (Alexander *et al.*, 2013) is intermediate between the Yew and Weng curve and the curve for the present study. The rough underside of the ice is made by band-pass filtering a Gaussian random variable that is scaled such that the underside never has a slope greater the 7 deg. The mean ice thickness is 1.2 m. the thickness standard deviation is 0.1 m, and the filter passes horizontal wavelengths between 4 and 100 m. The intent of the rough ice layer is to absorb and scatter sound in a manner similar to ice cover, not to examine the precise details of ice scattering. Figure 1(b) shows results obtained using these parameters. Despite the reflection coefficient being larger than the example estimate that is cited (Yew and Weng, 1987), the complex-density layer with a gently sloped underside (no ice keels) absorbs sufficient sound and sends sufficient sound into the seabed to mimic the strong attenuation observed with ice cover.

Figure 1(b) shows the intensity from a source with source level (SL) of 0 dB as a function of range for approximately current *p*H conditions and flat open-water conditions. For the computation, the *in situ* *p*H is set at 8.1 throughout the water column, a simplification of historic conditions that are more commonly measured at the surface (Ciais *et al.*, 2013) and have time-variable and depth-variable profiles (Shadwick *et al.*, 2011; AMAP, 2013). The computations confirm the expected results: sound in the duct undergoes cylindrical spreading, and peak pulse levels in the duct with no ice and a flat surface are slightly higher than they are with ice because non-ducted sound energy moving at the same horizontal rate as the ducted sound is added to the ducted sound. The non-ducted sound energy will be disregarded in the remainder of this paper. The modeling shows that intensity of sound in the duct can be approximated by

$$I(r) = \mathrm{SL} - 20\log_{10}(R_s) - 10\log_{10}(r/R_s) - \alpha(T,S,p,p\mathrm{H})r, \quad (1)$$

where the spherical spreading radius R_s is 14 m. The absorption coefficient α is a function of the temperature, salinity, pressure and *p*H of the water. For propagation in the duct, parameter values of −1.322, 32.387, 112, and either 7.9 or 8.1 for *p*H were used, respectively. The $R_s = 14$ m value is smaller than $R_s = 35$ m used by Lovett (1975) for deep-ocean sound-channel propagation, where the primary duct is wider. Expression (1) loses accuracy at low frequency where no sound is confined within the duct. The *p*H dependence of α causes $I(r)$ to be *p*H dependent. The final term is a constant-α approximation of $\int \alpha_D(r)dr$ that is sufficient for propagation in the relatively stable duct, where α_D is the average α over the depth of the duct at any given range.

III. ANTICIPATED FUTURE *p*H AND ABSORPTION

One published prediction shows Arctic Ocean surface *p*H decreasing from 8.1 in 2000 to 7.9 in about 2050, and further to 7.7 in about 2085 (Ciais *et al.*, 2013). The likely reduction is supported by some basic facts about the circulation in this area. PSW and PWW originating in the shallow

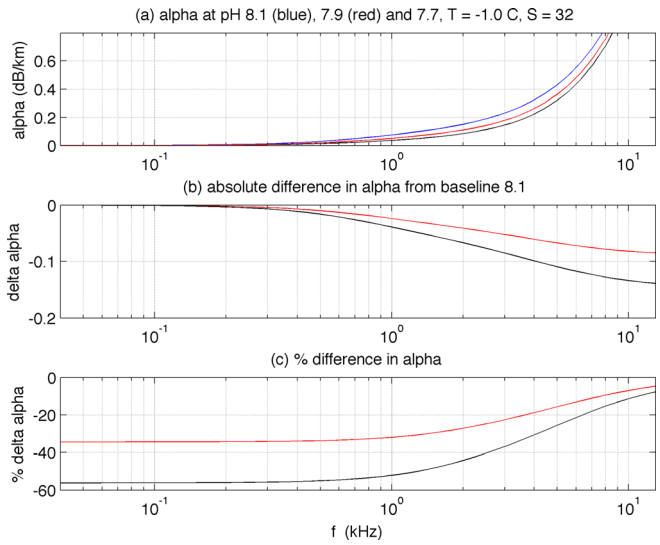

FIG. 3. (Color online) (a) Absorption α with units dB/km is plotted at zero pressure for temperature $-1.0\,^{\circ}$C, salinity 32 g/kg and three different pH levels. (b) The differences between pairs of α curves in (a) are plotted. (Red) The $p\mathrm{H}=7.9$ minus the $p\mathrm{H}=8.1$ curve. (Black, lower line) The $p\mathrm{H}=7.7$ minus the $p\mathrm{H}=8.1$ curve. (c) The percentage reduction computed for the curves shown in (a) and (b).

Bering Strait, Chukchi Sea, and Barrow Canyon areas (Pickart *et al.*, 2005; Itoh *et al.*, 2012) are subject to strong atmospheric exchange processes (ventilation) and are likely to absorb carbon dioxide and thus show declining future pH. After flowing northward into the Beaufort Sea/Canada Basin, the relatively high rate of horizontal diffusivity commonly found in the ocean that may be enhanced by atmospheric-event (storm, wind event) forced eddies (Schulze and Pickart, 2012; Pickart *et al.*, 2013) is likely to cause the low pH ionic conditions to permeate most or all of the Pacific Water in the area. Diapycnal diffusion is weak in this area (Timmermans *et al.*, 2008), so the pH alteration above and below the Pacific water may lag. Figure 3 shows absorption $\alpha(T, S, p, p\mathrm{H})$ at three pH levels across a wide frequency band, with one temperature T, one salinity S, and one pressure p value used in the illustrative plots, with parameters chosen to represent duct propagation. The calculations are made using the relaxation absorption expressions of Brewer *et al.* (1995) and the viscous absorption expression of Francois and Garrison (1982b); the viscous contribution is near zero at the frequencies shown. The percent reduction is highest at the low frequencies, but the difference in absorption is greatest at the highest frequencies. In the center of the band the net effects of the pH reduction are the most significant, shown in Sec. IV.

IV. COMPARING PRESENT AND FUTURE PROPAGATION

Figure 4 shows results obtained from the PE (with rough ice cover) and the simple model (1) for 900 Hz under two pH profile conditions, using the sound-speed profile of Fig. 1, with the source at 110 m depth. The baseline pH condition is taken to be 8.1 throughout the water column. [Robbins *et al.* (2013) report median surface pH of 8.05 in the Beaufort Sea in 2011.] The future condition case has a pH anomaly added that is linear in depth, is zero at the bottom (4000 m), and is -0.2 at the surface (i.e., the surface pH is 7.9). Calculations were made with other pH profiles such as one with the low-pH anomaly confined to the duct and above, but these give very similar results for sound in the duct, and the key finding is that (1) describes sound intensity in the duct when absorption α for pH, T, and S conditions in the duct is used. Once validated, the simple propagation model (1) was applied to many frequencies by simply changing α. Disregarding the deep nulls that are an artifact of the monochromatic PE calculations, a basic observation is that, at lower pH, sound travels further before dropping to any specific sound pressure level (SPL) than it does at higher pH.

Figure 5 shows results obtained with (1) for many frequencies. At the top, the percentage increase in distance, at reduced pH, that sound is predicted to travel before the SPL drops to a specific value is contoured in 2.5% increments. The percentage is calculated as 100 times $r_1(r_0,f)/r_0$, where $r_1(r_0,f)$ is the range at which SPL at frequency f at $p\mathrm{H}=7.9$ falls to its value at the shorter range r_0 at $p\mathrm{H}=8.1$, i.e., $\mathrm{SPL}_{7.9}(r_1,f)=\mathrm{SPL}_{8.1}(r_0,f)$. Figure 4 illustrates the calculation of this increase in distance. In Fig. 5, the increase in distance, as a percentage value 100 $r_1(r_0,f)/r_0$, is contoured at the top as a function of f and r_0. For sound pressure levels less than -90 dB re the source the background is white, indicating that low-level sound is being considered. The greatest

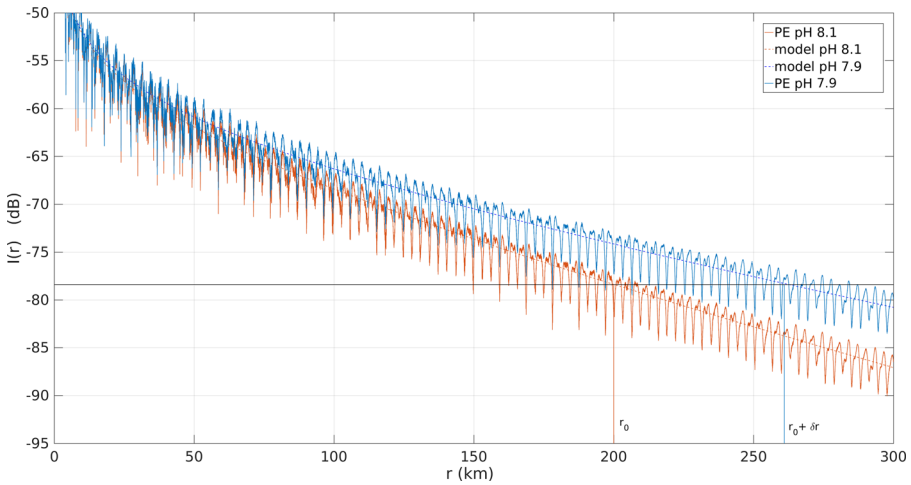

FIG. 4. (Color online) Parabolic equation output, with rough ice cover, is shown for 900-Hz sound at 110-m depth in the duct for two pH values, with everything else being equal. The outputs for the simple model (1) are also shown with dotted lines, these lack the modal interference patterns of the PE output. It can be seen that sound at pH 7.9 has higher level than sound at pH of 8.1. This means that sound traveling distance r_0 at pH 8.1 will have the same level at the distance $r_0+\delta r$ with pH 7.9, or equivalently will travel $100[(r_0+\delta r)/r_0]$ percent further.

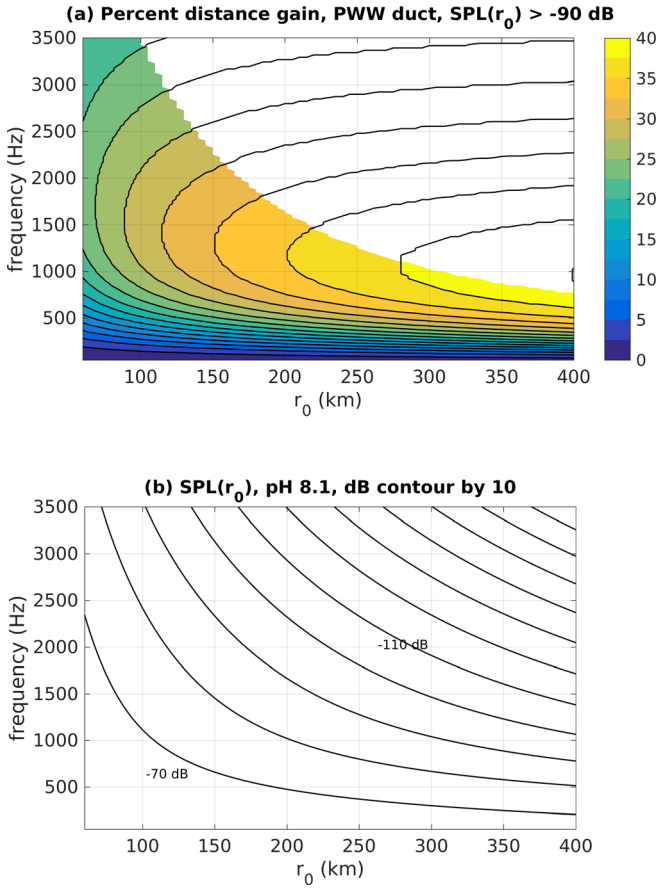

FIG. 5. (Color online) (a) The percent extra distance gained due to a *p*H reduction from 8.1 to 7.9 for sound in the duct, with a source in the duct, is shown as a function of frequency and distance from source r_0. The values are contoured with filled color for $SPL_{8.1}(r_0) > -90$ dB at *p*H 8.1 for a 0 dB level source [i.e., $TL(r_0) < 90$ dB]. For lower SPL (weak signal) the color is omitted. The extra distance exceeds 38% at long distances near 1000 Hz. (b) A contour plot of $SPL_{8.1}(r_0,f)$ is shown.

distance gained is for frequencies centered at 1000 Hz at distances over 280 km. This is exactly in the operating range of the cited acoustic research navigation system.

There are a few possible sources of uncertainty in the quantities shown in Fig. 5. One is that R_s may be frequency dependent because the duct-trapped mode quantity will increase with frequency, distorting the SPL shown in Fig. 5(b). (On the other hand, the ratio of trapped mode quantity to total mode quantity will not change greatly. Also note that R_s of 14 m at 900 Hz is related to three modes being trapped in the duct, tabulated by normal mode analysis of the Fig. 1(a) sound speed profile.) Such R_s dependence is presumed to be small over the band 500−3500 Hz and is not considered here. Running the model with a wide range of R_s values changes SPL [Fig. 5(b)] by only a few dB and does not change the character of Fig. 5(a). Also, note that the influence R_s of cancels out when comparing results at different *p*H at any single frequency, our primary result. The neglect of the frequency-dependence of R_s will produce insignificant errors in SPL plotted as a function of range and frequency. These errors and uncertainties are small compared to uncertainties of the duct sound-speed profile and possible range-dependence of the duct. Quantifying such details of the ducted propagation as a function of frequency, time, and space is outside the scope of this paper.

V. A NOISE MODEL

Noise at 1000 Hz in the Beaufort Sea is unlikely to be affected by reduced *p*H in the same way as sound intentionally put into the duct. This is because the surface-generated sound suffers a greater fraction of its total attenuation via spherical spreading as it penetrates to deep water and via loss from repeated surface interaction. Some of the surface-generated sound will transit the PWW duct as is cycled to deeper water and back, but will not be trapped in the duct.

To quantify *p*H effect on noise detected in the duct (but not trapped there), a model of 1000-Hz noise is constructed using the concept of a distributed collection of sources (Kuperman and Ingenito, 1980). Multiple realizations of noise power at a single receiver are constructed as the incoherent sum of sound from sources placed at the surface at randomly selected locations. The mean and standard deviations of the sums from the many realizations form the output statistics of the noise model. Two sound intensity levels are produced for each realization, one made with absorption valid for *p*H 8.1 and one with absorption for *p*H 7.9. Sound intensity N at the imagined receiver from each source in each realization is computed using (1) with $R_s = 50$ m for surface noise in place of the 14-m value used for signal analysis in the duct, where the computed quantity $N(r)$ is written in place of intensity $I(r)$. For each realization, 100 sources are placed randomly (selected from uniform distributions in x and y) in a 40-km by 40-km square with the receiver at the center. A probability distribution of source level (SL) is also used in the model; SL for each source is randomly selected from a log-normal distribution. A wide selection of SL mean and SL standard deviation choices were used. These spatial distribution and SL distribution parameters were chosen with guidance from Kinda *et al.* (2013) and Kinda *et al.* (2015) who recorded noise statistics in the Beaufort Sea. No exhaustive effort was made to exactly match the graphical and tabular noise statistics published in those papers; discrepancies between the published noise statistics and the statistics of the noise model are evaluated in the next paragraph. Using temperature −1.3 °C and $S = 32$, absorptions are $\alpha_{8.1} = 7.49 \times 10^{-5}$ dB/m for *p*H = 8.1, and then $\alpha_{7.9} = 5.10 \times 10^{-5}$ dB/m for *p*H = 7.9, i.e., two sound power levels at the receiver, called $n_{8.1}$ and $n_{7.9}$, are computed for each source. As for notation, the modeled noise power results are the sums $N_m = \Sigma n_m$ of the 100 sources of each realization, where $m = 8.1$ or 7.9.

One version of the model uses SL mean 80 dB and standard deviation 16 dB. Figure 6 shows two aspects of this modeled noise, the histogram of $N_{8.1}$ and the histogram of $N_{7.9}$ - $N_{8.1}$, with means and standard deviations listed. In the model run (6000 realizations), the quietest noise, with only distant sources, has a 0.7 dB increase for the lower *p*H. The loudest noise, which occurs in realizations where a loud source is close by, is increased by less that 0.4 dB. Noise realizations with intermediate $N_{8.1}$ can increase from 0 to 1.2 dB depending on whether they are dominated by close sources or by distant but very loud sources. Using the SL

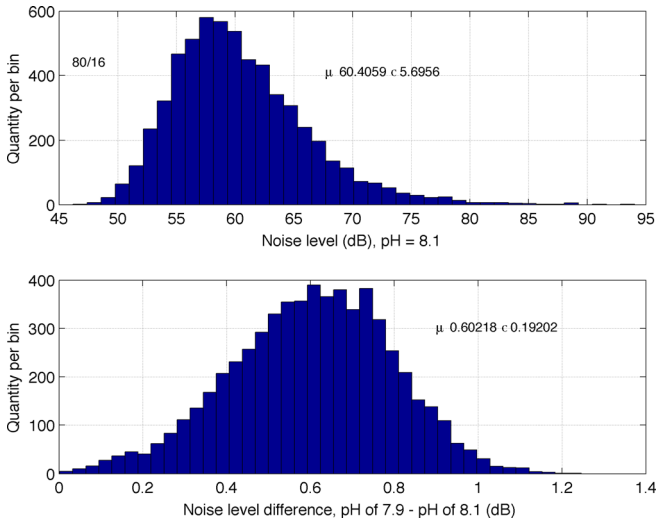

FIG. 6. (Color online) (Top) For the case of SL mean 80 dB and SL standard deviation 16 dB, the histogram of $N_{8.1}$ (in dB) for 6000 realizations is shown. (Bottom) The histogram of $N_{7.9} - N_{8.1}$ is shown. The means and standard deviations of each computed quantity are written.

mean/standard deviation parameters of 80/16 dB, the mean modeled $N_{8.1}$ is few dB above what Kinda *et al.* (2013) report. Kinda *et al.* (2015) report a few large transients of 130 dB that we cannot duplicate with this log-normal noise model, even after varying the parameters. Another SL distribution model such as a mixture model may better match the data, but the current log-normal model appears to be sufficient to show that 1000-Hz noise would increase slightly with a *p*H reduction from 8.1 to 7.9.

To explore whether this model could replicate the statistics of the Kinda *et al.* papers, and to fine-tune the *p*H-induced noise alteration estimate, the SL distributions were varied over a wide range. Figure 7 shows how the mean noise level, the noise standard deviation, the peak noise level, and the mean noise difference between the two *p*H cases vary with respect to SL log-normal distribution parameters. The mean 80 dB, standard deviation 16 dB case of Fig. 6 is one of the cases. A key result [Fig. 7(d)] is that the mean noise increase of just over 0.5 dB for the lower *p*H situation is not sensitive to the SL parameters.

The physical reason that the predicted increase (under reduced *p*H) of noise intensity level is smaller than the predicted increase of identified-source intensity level (signal level) for sources hundreds of km distant is that the noise is dominated by a few nearby events, particularly when the noise is at the highest observed dB level. Because the sounds in the noise field have not propagated far, the *p*H-change induced alteration in their level, given by $\Delta I = \int(\alpha_{7.9} - \alpha_{8.1})ds$, is not great. The small increases of noise shown in the lower portion of Fig. 6 are in agreement with the work of Joseph and Chiu (2010), Reeder and Chiu (2010), and Udovydchenkov *et al.* (2010), despite the differences between temperate propagation conditions used there and Beaufort Sea conditions used here. Running this noise model at 400 Hz after adjustments to match the noise levels of Kinda *et al.* (2013) at that frequency predicts less future enhancement of 400 Hz noise than of 1000 Hz noise, as expected.

VI. SNR

Changes to the ratio of signal in the duct to noise can now be computed from the predictions of signal change (Sec. IV) and noise change (Sec. V). The signal change was not given in dB, so one more operation is needed: the ratio $\mathrm{SPL}_{7.9}(r_0, f)/\mathrm{SPL}_{8.1}(r_0, f)$ must be computed. This is plotted

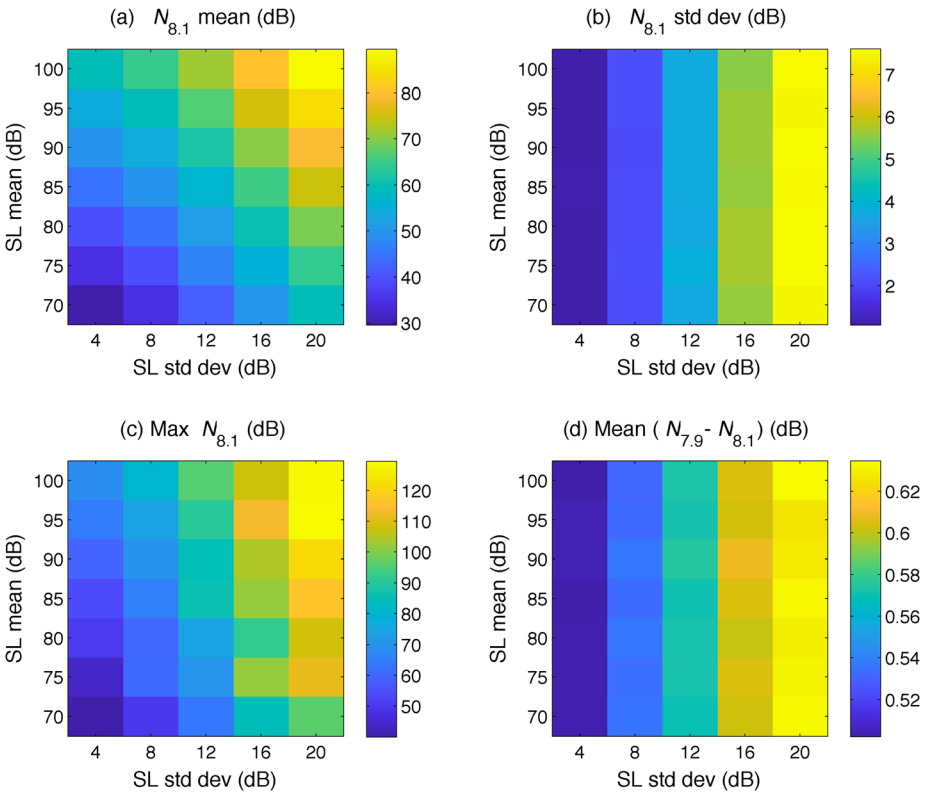

FIG. 7. (Color online) Statistics of noise are given for many choices of SL log-normal distribution, quantified in terms of SL mean and SL standard deviation, with each given in decibels. The SL distribution parameters are given in the axis labels. (a) Mean noise level at *p*H of 8.1. (b) Standard deviation of noise at *p*H of 8.1. (c) Maximum noise level at *p*H of 8.1. (d) Mean difference of noise level between the two *p*H cases, with noise levels for *p*H of 7.9 higher than levels for *p*H of 8.1.

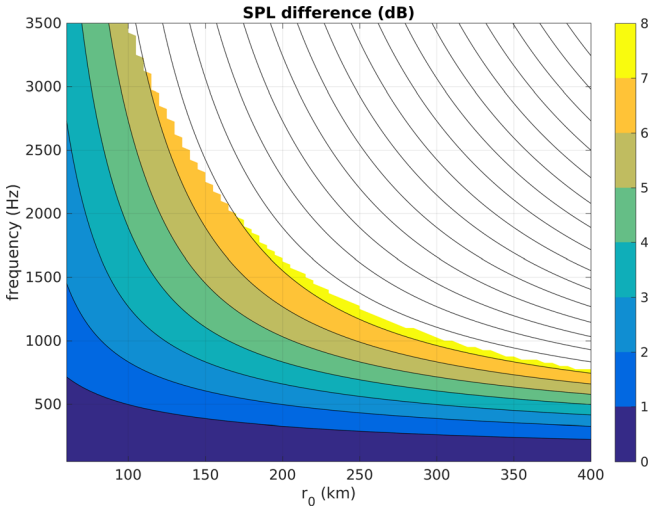

FIG. 8. (Color online) The difference $\Delta S(r_0, f) = S_{7.9}(r_0, f) - S_{8.1}(r_0, f)$ (both in dB) of sound in the duct is contoured. Contours from 1 to 22 dB are shown with black lines. Results for $SPL_{8.1}(r_0, f) > -90$ dB are filled with color, spanning 0 to over 7 dB.

in decibels in Fig. 8. The plot shows a 0−10 dB increase at 1000 Hz under the future conditions. Coupling this with the (much lower) 0.5 dB increase in noise modeled in Sec. V suggests that SNR in the duct will increase substantially in the future if the *p*H declines as projected.

VII. SUMMARY

A few circumstances unique to the Beaufort Sea suggest that *p*H changes to those waters that may occur in the future may strongly affect acoustic conditions. The existence of a subsurface duct there mitigates attenuation due to scattering from rough ice, and lets sound in the 1 kHz range travel far enough for absorption to have meaningful effect. This means that changes in absorption caused by *p*H changes may have measurable effects. It is predicted that signals emitted in the duct at ∼150 m depth will travel further by up to 40%, or equivalently, will have SPL increases of up to 7 dB at 200 km or greater distance from the source. Surface generated noise would not be trapped in the duct and would rise by a smaller amount, giving higher SNR for sound intentionally fed into the duct. One way to understand this effect is to realize that the highest-level noise events are consistent with sound generated nearby that does not travel far; absorption changes will have minimal effect on this sound.

The rate of change of Beaufort Sea *p*H is not at all certain. The future appearance of the duct-*p*H reduction scenario that is examined here is supported by the fact that the Pacific Winter Water is ventilated to the atmosphere and will equilibrate with an atmosphere of increasing carbon dioxide concentration. The relatively isolated (poorly ventilated) Atlantic Water below the duct may have more stable *p*H, in part because of low diapycnal mixing in this area (Timmermans *et al.*, 2008).

ACKNOWLEDGMENTS

The author thanks Lori Adornato of SRI for introduction to the issue of Arctic Ocean acidity and for important discussions of past, present, and future acidity conditions in the Arctic. Robert Byrne of the University of South Florida is also thanked for his input. Lee Freitag of WHOI is thanked for sharing information about under ice AUV acoustic navigation systems. The version of the RAM parabolic equation code implemented in Matlab by Matt Dzieciuch was modified then used for this work. Adopting the recommendations of the reviewers improved the article and they are thanked. This work was supported by Office of Naval Research Grant N00014-16-1-2372.

Alexander, P., Duncan, A., Bose, N., and Smith, D. (**2013**). "Modelling acoustic transmission loss due to sea ice cover," Acoust. Aust. **41**, 79–87; available at http://hdl.handle.net/20.500.11937/23321.

AMAP (**2013**). "AMAP Assessment 2013: Arctic Ocean Acidification. Arctic Monitoring and Assessment Programme (AMAP)," Oslo, Norway, viii + 99 pp.

Brewer, P. G., Glover, D. M., Goyet, C., and Shafer, D. K. (**1995**). "The pH of the North Atlantic Ocean: Improvements to the global model for sound absorption," J. Geophys. Res. **100**, 8761–8776, doi:10.1029/95JC00306.

Brewer, P. G., and Hester, K. (**2009**). "Ocean acidification and the increasing transparency of the ocean to low-frequency sound," Oceanography **22**(4), 86–93.

Caldeira, K., and Wickett, M. E. (**2005**). "Ocean model predictions of chemistry changes from carbon dioxide emissions to the atmosphere and ocean," J. Geophys. Res. **110**, C09S04, doi:10.1029/2004JC002671.

Ciais, P., C. Sabine, C., Bala, G., Bopp, L., Brovkin, V., Canadell, J., Chhabra, A., DeFries, R., Galloway, J., Heimann, M., Jones, C., Le, Quéré, C., Myneni, R. B., Piao, S., and Thornton, P. (**2013**). "Carbon and other biogeochemical cycles," in *Climate Change 2013: The Physical Science Basis. Contribution of Working Group I to the Fifth Assessment Report of the Intergovernmental Panel on Climate Change*, edited by T. F. Stocker, D. Qin, G.-K. Plattner, M. Tignor, S. K. Allen, J. Boschung, A. Nauels, Y. Xia, V. Bex, and P. M. Midgley (Cambridge University Press, Cambridge, UK).

Doney, S. C., Fabry, V. J., Feely, R. A., and Kleypas, J. A. (**2009**). "Ocean acidification: The other CO_2 problem," Ann. Rev. Mar. Sci. **1**(1), 169–192.

Feely, R. A., Sabine, C. L., Lee, K., Berelson, W., Kleypas, J., Fabry, V. J., and Millero, F. J. (**2004**). "Impact of anthropogenic CO2 on the CaCO3 system in the oceans," Science **305**, 362–366.

Francois, R. E., and Garrison, G. R. (**1982a**). "Sound absorption based on ocean measurements. Part II: Boric acid contribution and equation for total absorption," J. Acoust. Soc. Am. **72**(6), 1879–1890.

Francois, R. E., and Garrison, G. R. (**1982b**). "Sound absorption based on ocean measurements: Part I: Pure water and magnesium sulfate contributions," J. Acoust. Soc. Am. **72**(3), 896–907.

Freitag, L., Ball, K., Partan, J., Koski, P., and Singh, S. (**2015**). "Long range acoustic communications and navigation in the Arctic," in *Proceedings of Oceans 2015*, Washington, IEEE/MTS.

Hester, K. C., Peltzer, E. T., Kirkwood, W. J., and Brewer, P. G. (**2008**). "Unanticipated consequences of ocean acidification: A noisier ocean at lower *p*H," Geophys. Res. Lett. **35**, L19601, doi:10.1029/2008GL034913.

Itoh, M., Shimada, K., Kamoshida, T., Mclaughlin, F., Carmack, E., and Nishino, S. (**2012**). "Interannual variability of Pacific Winter Water inflow through Barrow Canyon from 2000 to 2006," J. Oceanogr. **68**, 575–592.

Joseph, J. E., and Chiu, C.-S. (**2010**). "A computational assessment of the sensitivity of ambient noise level to ocean acidification," J. Acoust. Soc. Am. **128**, EL144–EL149.

Kinda, G. B., Simard, Y., Gervaise, C., Mars, J. I., and Fourtier, L. (**2013**). "Under-ice ambient noise in Eastern Beaufort Sea, Canadian Arctic, and its relation to environmental forcing," J. Acoust. Soc. Am. **134**(1), 77–87.

Kinda, G. B., Simard, Y., Gervaise, C., Mars, J. I., and Fortier, L. (**2015**). "Arctic underwater noise transients from sea ice deformation: Characteristics, annual time series, and forcing in Beaufort Sea," J. Acoust. Soc. Am. **138**(4), 2034–2045.

Kuperman, W. A., and Ingenito, F. (**1980**). "Spatial correlation of surface generated noise in a stratified ocean," J. Acoust. Soc. Am. **67**(6), 1988–1996.

Lovett, J. R. (**1975**). "Northwestern pacific sound attenuation using low-frequency CW sources," J. Acoust. Soc. Am. **58**, 620–625.

Pickart, R. S. (**2004**). "Shelfbreak circulation in the Alaskan Beaufort Sea: Mean structure and variability," J. Geophys. Res. **109**, C04024, doi:10.1029/2003JC001912.
Pickart, R. S., Pratt, L. J., Zimmermann, S., and Torres, D. J. (**2005**). "Flow of winter-transformed water into the western Arctic," Deep-Sea Res. II **52**, 3175–3198.
Pickart, R. S., Spall, M. A., and Mathis, J. T. (**2013**). "Dynamics of upwelling in the Alaskan Beaufort Sea and associated shelf–basin fluxes," Deep-Sea Res. I **76**, 35–51.
Reeder, D. B., and Chiu, C.-S. (**2010**). "Ocean acidification and its impact on ocean noise: Phenomenology and analysis," J. Acoust. Soc. Am. **128**, EL137–EL143.
Robbins, L. L., Wynn, J. G., Lisle, J. T., Yates, K. K., Knorr, P. O., Byrne, R. H., Liu, X., Patsavas, M. C., Azetsu-Scott, K., and Takahashi, T. (**2013**). "Baseline monitoring of the western Arctic Ocean estimates 20% of Canadian Basin surface waters are undersaturated with respect to aragonite," PLoS ONE **8**(9), e73796.
Schulze, L. M., and Pickart, R. S. (**2012**). "Seasonal variation of upwelling in the Alaskan Beaufort Sea: Impact of sea ice cover," J. Geophys. Res. **117**, C06022, doi:10.1029/2012JC007985.
Shadwick, E. H., Thomas, H., Chierici, M., Else, B., Fransson, A., Michel, C., Miller, L. A., Mucci, A., Niemi, A., Papakyriakou, T. N., and Tremblay, J.-É. (**2011**). "Seasonal variability of the inorganic carbon system in the Amundsen Gulf region of the southeastern Beaufort Sea," Limnol. Oceanogr. **56**, 303–322.
Spall, M. A., Pickart, R. S., Fratantoni, P. S., and Plueddemann, A. J. (**2008**). "Western Arctic shelfbreak eddies: Formation and transport," J. Phys. Oceanogr. **38**, 1644–1668.
Timmermans, M.-L., Toole, J., Krishfield, R., and Winsor, P. (**2008**). "Ice-tethered profiler observations of the double-diffusive staircase in the Canada Basin thermocline," J. Geophys. Res. **113**, C00A02, doi:10.1029/2008JC004829.
Udovydchenkov, I. A., Duda, T. F., Doney, S. C., and Lima, I. D. (**2010**). "Modeling deep ocean shipping noise in varying acidity conditions," J. Acoust. Soc. Am. **128**, EL130–EL136.
Webster, S. E., Freitag, L. E., Lee, C. M., and Gobat, J. I. (**2015**). "Towards Real-Time Under-Ice acoustic navigation at mesoscale ranges," in *Proceedings of IEEE Intl. Conf. Robot. Auto.*, Seattle.
Woods Hole Oceanographic Institution (**2007**). "Ice tethered profiler: An autonomous instrument for sustained observation of the Arctic Ocean," http://www.whoi.edu/website/itp/ (Last viewed 29 August 2017).
Yew, C. H., and Weng, X. (**1987**). "A study of reflection and refraction of waves at the interface of water and porous sea ice," J. Acoust. Soc. Am. **82**, 342–353.
Zhang, Z. Y., and Tindle, C. T. (**1995**). "Improved equivalent fluid approximations for a low shear speed ocean bottom," J. Acoust. Soc. Am. **98**, 3391–3396.